Computerized Medical Imaging and Graphics 33 (2009) 317–324

Contents lists available at ScienceDirect

Computerized Medical Imaging and Graphics

journal homepage: www.elsevier.com/locate/compmedimag

Ultrasound image texture analysis of the intima and media layers of the common carotid artery and its correlation with age and gender

C.P. Loizou[a,*], M. Pantziaris[b], M.S. Pattichis[c,d], E. Kyriacou[e], C.S. Pattichis[f]

[a] Department of Computer Science, School of Sciences, Intercollege, P.O. Box 51604, CY-3507 Limassol, Cyprus
[b] Cyprus Institute of Neurology and Genetics, Nicosia, Cyprus
[c] Department of Electrical and Computer Engineering, University of New Mexico, Albuquerque, USA
[d] Department of Radiology, School of Medicine, University of New Mexico, Albuquerque, USA
[e] Department of Computer Science, Frederic University, Limassol, Cyprus
[f] Department of Computer Science, University of Cyprus, Nicosia, Cyprus

ARTICLE INFO

Article history:
Received 20 January 2009
Received in revised form 16 February 2009
Accepted 20 February 2009

Keywords:
Stroke
Ultrasound image
Texture analysis
Initma–media layer
Carotid artery
Media layer
Intima layer

ABSTRACT

The intima–media thickness (IMT) of the common carotid artery (CCA) is widely used as an early indicator of cardiovascular disease (CVD). It was proposed but not thoroughly investigated that the composition and texture of the media layer (ML) can be used as an indicator for the risk of stroke. In this study, we investigate the application of texture analysis of the ML of the CCA and how texture is affected by age and gender. The study was performed on 100 longitudinal-section ultrasound images acquired from asymptomatic subjects at risk of atherosclerosis. The images were separated into three different age groups, namely below 50, 50–60, and above 60 years old. Furthermore, the images were separated according to gender. A total of 61 different texture features were extracted from the intima layer (IL), the ML, and the intima–media complex (IMC). The ML and the IMC were segmented manually by a neurovascular expert and also automatically by a snakes segmentation system. We have found that male patients tended to have larger media layer thickness (MLT) values as compared to the MLT of female patients of the same age. We have found significant differences among texture features extracted from the IL, ML and IMC from different age groups. Furthermore, for some texture features, we found that they follow trends that correlate with a patient's age. For example, the gray-scale median GSM of the ML falls linearly with increasing MLT and with increasing age. Our findings suggest that ultrasound image texture analysis of the media layer has potential as an assessment biomarker for the risk of stroke.

1. Introduction

As reported by the World Health Organization cardiovascular disease (CVD; coronary artery disease, cerebrovascular disease and peripheral artery disease) is the third leading cause of death and adult disability in the industrial world after heart attack and cancer [1]. According to [1], 80 million American adults have one or more types of CVD of whom about half are estimated to be age 65 or older. Of all the deaths caused by CVD among adults aged 20 and older, an estimated 13 millions are attributed to coronary heart disease and to stroke, with atherosclerosis as the underlying cause. A recent study by the World Health Organization estimates that by 2015, 20 million people will die from cerebrovascular disease, mainly from heart attack and stroke.

Atherosclerosis causes enlargement of the arteries and thickening of the artery walls. Thus, clinically, the intima–media thickness (IMT) is used as a validated measure for the assessment of atherosclerosis [2] (see Fig. 1). It was proposed, but not thoroughly investigated, that not only the IMT but rather the ML (its thickness and its textural characteristics) may be used for evaluating the risk that a subject might develop stroke. The objective of this study is to investigate the application of texture analysis of IL, and ML of the common carotid artery (CCA), and how texture is affected by age and gender. Only three studies [3–5] investigated textural changes of the IMC, but not for the IL and ML separately (that are briefly presented below).

As shown in Fig. 1, the intima layer (IL) is a thin layer, the thickness of which increases with age, from a single cell layer at birth to 250 μm at the age of 40 for non-diseased individuals [6]. In ultrasound images, the media layer (ML) is characterized by an echolucent region, predominantly composed of smooth muscle cells, enclosed by the intima and adventitia layers (see

* Corresponding author. Tel.: +357 25 381180.
E-mail addresses: panloicy@logosnet.cy.net, loizou.c@lim.intercollege.ac.cy, loizou.christos@ucy.ac.cy (C.P. Loizou), pantzari@cing.ac.cy (M. Pantziaris), pattichis@ece.unm.edu (M.S. Pattichis), ekyriac@ucy.ac.cy (E. Kyriacou), pattichi@ucy.ac.cy (C.S. Pattichis).

0895-6111/$ – see front matter © 2009 Elsevier Ltd. All rights reserved.
doi:10.1016/j.compmedimag.2009.02.005

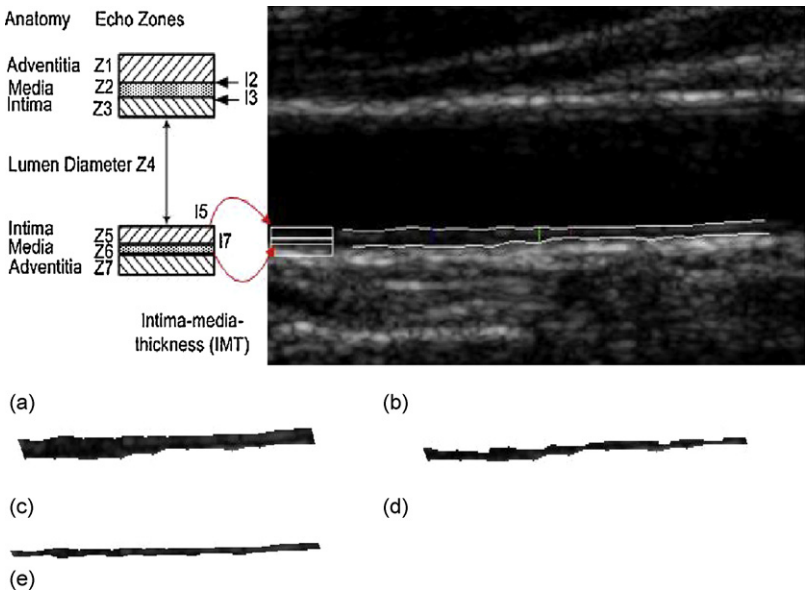

Fig. 1. (a) Illustration of the intima–media complex (IMC) of the far wall of the (b) common carotid artery and the automatic IMC segmentation [9,10,16]. The media layer (ML) is defined as the layer (band) between the intima–media and the media–adventitia interface (band Z6), (c) extracted IMC, (d) extracted media layer (ML) and (e) extracted intima layer (IL).

Fig. 1, band Z6) [2,7]. Earlier research [8] showed that the media layer thickness (MLT) does not change significantly with age ($125\,\mu m < MLT < 350\,\mu m$). In a recent study by our group, the median (IQR) of intima layer thickness (ILT), MLT, and IMT were computed from 100 ultrasound images of 42 female and 58 male asymptomatic subjects aged between 26 and 95 years old, with a mean age of 54 years to be as follows 0.43 mm (0.12), 0.23 mm (0.18), and 0.66 mm (0.18) respectively [9,10].

In [3] a method has been presented for quantifying the reflectivity of the ML of the distal CCA. It was shown that the GSM of the IM layer is the earliest change representing atherosclerotic disease in the arterial wall that can currently be imaged in vivo. This may be the first marker of atherosclerosis and may precede the development of a significant increase in IMT. This would enable earlier identification of high-risk individuals based on the analysis of the CCA artery wall textural characteristics. In [4], the early structural changes of the CCA in familial hypercholesterolemia were investigated. It was shown that textural characteristics extracted from the IMC were significantly different between patients with and without hypercholesterolemia. In [5], the authors reported on the properties of the GSM of the IMC from a random sample of 1016 subjects aged exactly 70. They found that the GSM of the IMC of the CCA is closely related to the echogenecity in overt carotid plaques.

While there are several earlier studies suggesting that the instability of the carotid atheromatous plaques can be characterized from B-mode ultrasound images [7,11], we have not found any other studies reported in the literature where the ML textural characteristics have been shown to be associated with the risk of stroke. While in [7] and [11], the echogenecity in atherosclerotic carotid plaques was evaluated through the gray-scale median (GSM) there are very few attempts made to characterize the IL, the ML and the intima–media complex (IMC) with a similar gray scale image intensity analysis. It is evident from the visual inspections of the IMC in the CCA that a great variation in echogenecity does exist. However, the usefulness of this information has not yet been studied.

In [11], the morphology of atherosclerotic carotid plaque was investigated based on the textural characteristic extracted from 230 ultrasound images of carotid plaque, where it was shown that it is possible to identify a group of patients, symptomatic or asymptomatic, at risk of stroke based on these texture features. It was further documented in [12], that carotid endarterectomy in asymptomatic individuals with stenosis grater than 70% reduces the risk of stroke from 2% per year to 1% per year. In another study [13] the relationship of the IMT in the CCA and atherosclerosis was investigated on 182 symptomatic patients (mean age 67 years). It was shown that the IMT was correlated to age, male gender, ischemic heart disease, and presence of plaque or stenosis in any of the carotid bifurcations. In a recent study [14], where the alterations of the CCA with age in ultrasound images were investigated, it was shown that the diastolic and systolic lumen diameters are increasing with age. This reduces wall stress as the elasticity of the wall decreases with age.

We propose to study changes in textural characteristics that can be associated with disease progression for different age groups. Here, we note that for fully developed plaques in the CCA, texture features derived from statistical, model based, and Fourier based methods, have been used to characterize and classify carotid atheromatous plaques from B-mode ultrasound images [11].

The objective of our study is to investigate whether textural characteristics extracted from the IL, the ML, and the IMC of the CCA, segmented manually by an expert and automatically by a snake's segmentation system [9,10] can be associated with the increase in age gender or MLT. Ultimately, texture feature characteristics that vary with age, gender or MLT might be used to assess the risk of stroke.

The paper is organized as follows. In Section 2, we provide materials and methods for the current study. Results are given in Section 3. We provide discussion in Section 4, and give concluding remarks in Section 5. To the best of our knowledge no other study carried out IL and ML ultrasound textural measurements for investigating their relationship with the increase of age, and the risk of stroke based on their textural characteristics. We do note that the best known (related) results were presented in [12,15], where it was shown that IMT increases linearly with age.

2. Materials and methods

2.1. Recording of ultrasound images

A total of 100 B-mode longitudinal ultrasound images of the CCA were recorded using the ATL HDI-3000 ultrasound scanner

(Advanced Technology Laboratories, Seattle, USA). For the recordings, a linear probe (L74) at a recording frequency of 7 MHz was used. Assuming a sound velocity propagation of 1550 m/s and 1 cycle per pulse, we thus have an effective spatial pulse width of 0.22 mm with an axial system resolution of 0.11 mm [16]. We use bicubic spline interpolation to resize all images to a standard pixel density of 16.66 pixels/mm (with a resulting pixel width of 0.06 mm).

The images were recorded at the Cyprus Institute of Neurology and genetics, in Nicosia, Cyprus, from 42 female and 58 male asymptomatic patients. Overall, patient's ages varied between 26 and 95 years old, with a mean age of 54 years. The images were partitioned into three different age groups. In the first group, we included 27 images from patients who were younger than 50 years old. In the second group, we had 36 patients who were 50–60 years old. In the third group, we included 37 patients who were older then 60 years old.

The subjects were at risk of atherosclerosis but they had not developed clinical symptoms, such as a stroke or a transient ischemic attack. Furthermore, the images were normalized as described in [17].

2.2. Manual measurements

A neurovascular expert manually segmented (using the mouse) the IL, ML layer [9,10] and the IMC [16] on each image after image normalization by selecting 20–40 consecutive points for the adventitia, media and intima at the far wall. The measurements were performed between 1 and 2 cm proximal to the bifurcation of the CCA, on the far wall [2], over a distance of 1.5 cm. The bifurcation of the CCA was used as a guide and all measurements were made with reference to that region. The IMT, MLT and the ILT were then calculated as the average of all vertical measurements taken at the interpolated perpendicular distances between these structures. The measuring points and delineations were saved for further comparison. All sets of manual segmentation measurements were performed by the expert in a blinded manner, both with respect to identifying the subject and as to the image automated segmentation.

2.3. IL, ML and IMC snake segmentations

All images were automatically segmented to identify the IL, ML and IMC regions. Automatic segmentation was carried out after image normalization using the snakes segmentation system proposed and evaluated on ultrasound images of the CCA in [9,10] and [16]. The segmentation system is based on the Williams and Shah method [18]. Using the definitions given in Fig. 1, we first segment the IMC [16] by extracting the I5 (lumen–intima interface) and the I7 boundaries (media–adventitia interface). The upper side of the ML (see Fig. 1, Z6) was then estimated by deforming the lumen–intima interface (boundary I5) by 0.36 mm (6 pixels) downwards and then deformed by the snakes segmentation algorithm proposed in [16] in order to fit to the media boundary. This displacement of 0.36 mm is based on the observation that the manual mean IMT lies between 0.54 mm (minimum of IMT_{mean}) and 0.88 mm (maximum of IMT_{mean}), with a mean IMT of 0.71 mm [16]. By taking into consideration that the spatial resolution (distance between two pixels) is 0.06 mm, then the IMT is lying within the range of 0.54–0.88 mm ($9 < IMT < 15$ pixels), with a mean of 0.71 mm (12 pixels). Therefore the displacement of the contour, in order to estimate the media should be on average 0.36 mm (6 pixels $\times$ 0.06 mm) downwards, which is half of the size of the IMT (the distance between I5 and I7, where I7 is the media–adventitia interface). In order to achieve standardization in extracting the thickness and texture measures from the IL, ML and IMC segments with similar dimensions, the following procedure was carried out. A region of interest of 9.6 mm (160 pixels) in length was first extracted. This was done by estimating the center of the IMC area and then selecting 4.8 mm (80 pixels) left and 4.8 mm (80 pixels) right of the center of the segmented IMC. Selection of the same ML length from each image is important in order to be able to extract comparable measurements between images and subject groups.

2.4. Texture analysis

In order to estimate textural characteristics extracted from the IL, ML and the IMC, a total of 61 different texture features were extracted both from the manual and the automated segmented regions of interest where only the most significant are presented. The following texture feature set algorithms were used: (i) statistical features [9,10]: (a) mean, (b) variance, (c) median value, (d) skewness, (e) kurtosis, (f) energy and (g) entropy. (ii) Spatial gray level dependence matrices (SGLDM) as proposed by Haralick et al. [19]: (a) angular second moment, (b) contrast, (c) correlation, (d) sum of squares variance, (e) inverse difference moment, (f) sum average, (g) sum variance, (h) sum entropy, (i) entropy, (j) difference variance, (k) difference entropy, and (l) information measures of correlation. For a chosen distance d (in this work $d = 1$ was used) and for angles $\theta = 0^\circ$, 45°, 90°, and 135°, we computed four values for each of the above texture measures. (iii) Gray level difference statistics (GLDS) [20]: (a) homogeneity, (b) contrast, (c) energy, (d) entropy, and (e) mean. The above features were calculated for displacements $\delta = (0, 1)$, $(1, 1)$, $(1, 0)$, $(1, -1)$, where $\delta \equiv (\Delta x, \Delta y)$, and their mean values were taken. (iv) Neighborhood gray tone difference matrix (NGTDM) [21]: (a) coarseness, (b) contrast, (c) busyness, (d) complexity, and (e) strength. (v) Statistical feature matrix (SFM) [22]: (a) coarseness, (b) contrast, (c) periodicity, and (d) roughness. (vi) Laws texture energy measures (LTEM) [22]: LL-texture energy from LL kernel, EE-texture energy from EE-kernel, SS-texture energy from SS-kernel, LE-average texture energy from LE and EL kernels, ES-average texture energy from ES and SE kernels, and LS-average texture energy from LS and SL kernels. (vii) Fractal dimension texture analysis (FDTA) [22]: the hurst coefficients for dimensions 4, 3 and 2 were computed. (viii) Fourier power spectrum (FPS) [22]: (a) radial sum and (b) angular sum.

2.5. Statistical analysis

The Mann–Whitney rank sum test (for independent samples of different sizes) was used in order to identify if there are significant differences (SD) or not (NS) between the extracted features. For significant differences, we require $p < 0.05$, and compare between age groups and between male and female patients. Similarly, for comparing independent samples from equal populations, we use the Wilcoxon rank sum test. We use the Wilcoxon rank sum test to detect texture feature differences between the IL, ML, and IMC, for both manual and automated segmentations. We use regression analysis to investigate the relationship between the gray-scale median (GSM) and age, between the GSM and MLT and between MLT and male and female patients.

3. Results

Table 1 presents the median and inter quartile range (IQR) of selected texture features extracted from the automated IL, ML, and IMC segmentations of the 100 ultrasound images investigated. From Table 1, we can see that most of the texture features extracted from the ML exhibit lower median and IQR values when compared with those extracted from the IL and IMC (e.g., mean, GSM, STD, contrast, ASM, coarseness).

Table 1
Texture features (median (IQR)) for the IL, ML, AND IMC using automated segmentations.

	IL	ML	IMC
Mean	35 (19.3)	21 (25)	33 (22)
GSM	35 (18.5)	28 (18)	30 (21.3)
STD	16 (6.6)	14 (7)	16 (5.7)
Contrast	52 (75)	28 (32)	61 (57)
DV	16 (27.8)	81 (56)	32 (32)
Complexity	1704 (3175)	6041 (6762)	4166 (5888)
ASM	0.09 (0.04)	0.002 (0.003)	0.003 (0.002)
Coarseness	20 (14.5)	13 (11)	24 (11.3)
SS-TEL	38 (33)	78 (53)	56 (38)
Entropy	5.7 (1.15)	6 (1.2)	6.6 (0.7)
Roughness	2.46(0.187)	2.2 (0.100)	2.238 (0.079)
Periodicity	0.8 (0.07)	0.9 (0.06)	0.8 (0.2)

IQR, inter-quartile-range; GSM, gray-scale median; STD, standard deviation; DV, difference variance; ASM, angular second moment; SS-TEL, SS-texture energy laws.

In Table 2, we use the Wilcoxon rank sum test to compare selected texture features extracted from automated and manual segmentations. We can see similar results for both manual and automated segmentations. However we note that there are differences. To avoid issues associated with segmentation differences, we are only interested in textural features that give significant differences for both manual and automated segmentations. For better visualization, we put these features in bold face (see Table 2). Between the IL and the ML, we have significant differences in 10 out of 11 features. Between IL and IMC, we have six texture features with significant differences. Similarly, we have eight texture features that exhibit significant differences between the IL and the ML in Table 3. We refer to Table 1 for a summary of the texture feature values.

Table 4 presents the Mann–Whitney rank sum test performed on selected texture features extracted from the automated IL, ML and IMC segmentations for the three different age groups. It is shown that some of the texture features (GSM, STD, DV, complexity, coarseness and SS-TEL) exhibit significantly different values between different age groups.

Fig. 2 presents box plots of the GSM texture features for the three different age groups. These measurements were extracted using the automated IL/ML/IMC segmentations.

Fig. 3 presents plots of the patient's GSM as a function of age and MLT. We use regression analysis to estimate linear relationships between GSM and age and between the GSM and the MLT. As a function of age (see Fig. 3a) the GSM has an estimated slope of 57.4 (S.E. of 13.7), with a correlation coefficient of $\rho = 0.12$. We estimated an F-ratio of 0.62 at a significance level of $p = 0.43$. The results provide quantitative evidence of a linear relationship between the GSM of the ML and the age of a subject. We present the plot of the GSM versus the MLT in Fig. 3b. Here, we are using manual measurements to estimate the MLT (also see Fig. 4).

Table 3
Texture characteristics of IL versus ML based on the texture feature values given in Table 1.

Corresponding features from Table 1	IL	ML
Mean, GSM	Brighter	Darker
Contrast, ASM	Higher contrast	Less contrast
Complexity, entropy	Low complexity	High complexity
Coarseness	More coarse, i.e. large areas with small gray tone variations	Less coarse, i.e. less local uniformity in intensity
Roughness	Slightly rougher	Smoother
Periodicity	Less periodical, more heterogeneous	More periodical, more homogeneous

In Table 5, we compare textural differences associated with differences in gender. We present the results from applying the Mann–Whitney rank sum test on selected texture features extracted from the automated IL, ML, and IMC segmentations for the male and female patients. We note that many significant differences were found between textural features associated with the IMC.

We present plots of the GSM as a function of the MLT in Fig. 4. For the male subjects, we had a slope of 50.82 (S.E. of 22.23), an axis intercept of 63.83 (S.E. of 6.98) and a correlation coefficient of $\rho = -0.29$. We estimated an F-ratio of 5.22 at a significance level of $p = 0.026$. The results provide evidence of a linear relationship between the age of male subjects and the MLT. It is shown that the GSM of the male subjects at an MLT of 0.3 mm is 60. Similarly, Fig. 4b presents the results for the female subjects. Here, we have a lower slope value of 18.92 (S.E. of 23.83) with an axis intercept of 45.06 (S.E. of 6.69) and a correlation coefficient of $\rho = 0.13$. The results gave an F-ratio of 0.63 at a significance level of $p = 0.43$. At a thickness of 0.3 mm the GSM was found to be 45.

We have also found that that there are some texture features (DV, entropy) which increase linearly with age, while others (GSM) decrease linearly for all measurements of the IL, ML and IMC. The correlation coefficients were estimated as: (a) $\rho = 0.13$ between GSM of ML and IL, (b) $\rho = 0.18$ between GSM of IMC and MT and (c) $\rho = 0.04$ between the GSM of IMC and IL. The strongest relationship is between the GSM of MLT and IMC.

4. Discussion

It was found (see Table 3) that the ML is less dark, has less contrast, is more periodic and is less coarse compared to IL. We have

Table 2
Wilcoxon rank sum comparison tests performed on texture features (first column) extracted from The IL, ML, and IMC using manual (M) automated (A) segmentations. In bold face, we have the texture features identified by the automated segmentation method that also exhibit significant differences for manual segmentation.

	Manual (M)			Automated (A)		
	IL-ML	IL-IMC	ML-IMC	IL-ML	IL-IMC	ML-IMC
Mean	S (0.01)	NS (0.5)	S (0.001)	**S (0.02)**	NS (0.81)	**S (0.004)**
GSM	NS (0.39)	NS (0.62)	S (0.001)	NS (0.3)	NS (0.45)	**S (0.04)**
Stand. dev.	S (0.01)	S (0.001)	S (0.001)	**S (0.001)**	NS (0.1)	**S (0.001)**
Contrast	S (0.001)	S (0.001)	S (0.001)	**S (0.001)**	NS (0.23)	**S (0.001)**
Diff. var.	S (0.001)	S (0.001)	S (0.01)	**S (0.001)**	**S (0.007)**	NS (0.09)
Complexity	S (0.001)	S (0.001)	S (0.04)	**S (0.001)**	**S (0.001)**	NS (0.09)
ASM	NS (0.3)	S (0.001)	NS (0.13)	**S (0.004)**	**S (0.001)**	**S (0.001)**
Coarseness	S (0.001)	S (0.021)	S (0.001)	**S (0.001)**	**S (0.005)**	**S (0.001)**
SS-TEL	S (0.009)	S (0.009)	NS (0.13)	**S (0.001)**	**S (0.02)**	NS (0.18)
Entropy	S (0.017)	S (0.001)	NS (0.85)	**S (0.001)**	**S (0.001)**	**S (0.008)**
Periodicity	S (0.001)	NS (0.92)	S (0.001)	**S (0.001)**	NS (0.07)	**S (0.02)**

IL, intima layer; ML, media layer; IMC, intima–media complex. The p-value is shown in parentheses (S = significantly different at $p < 0.05$, NS = non-significantly different at $p \geq 0.05$).

Table 4
Statistical comparisons between texture features extracted from the IL, ML, and IMC for different age groups. Here we use automated (first row) and manual (second row) segmentations. Statistical comparisons were based on the Mann–Whitney rank sum test for the three different age groups. Automated and manual IL, ML, and IMC segmentation measurements in mm (last row).

	IL			ML			IMC		
	<50	50–60	>60	<50	50–60	>60	<50	50–60	>60
Automated and manual segmentation measurements									
GSM									
<50		NS (0.3)	NS (0.3)		**S (0.01)**	**S (0.003)**		NS (0.08)	**S (0.03)**
		NS (0.23)	NS (0.23)		**S (0.02)**	**S (0.03)**		NS (0.43)	**S (0.03)**
50–60			NS (0.22)			NS (0.25)			NS (0.22)
			NS (0.11)			**S (0.01)**			NS (0.26)
STD									
<50		NS (0.36)	**S (0.01)**		NS (0.55)	**S (0.04)**		NS (0.65)	**S (0.03)**
		NS (0.33)	**S (0.03)**		NS (0.09)	**S (0.004)**		NS (0.23)	**S(0.04)**
50–60			NS (0.11)			NS (0.08)			NS (0.06)
			NS (0.3)			NS (0.07)			NS (0.3)
Contrast									
<50		NS (0.92)	**S (0.001)**		NS (0.7)	NS (0.8)		NS (0.3)	NS (0.25)
		NS (0.56)	**NS (0.01)**		NS (0.26)	NS (0.76)		**S (0.04)**	NS (0.06)
50–60			NS (0.55)			NS (0.55)			S (0.22)
			NS (0.3)			NS (0.22)			S (0.5)
DV									
<50		NS (0.33)	NS (0.87)		NS (0.18)	**S (0.01)**		NS (0.55)	**S (0.04)**
		NS (0.45)	NS (0.73)		NS (0.19)	NS (0.63)		**S (0.03)**	**S(0.02)**
50–60			NS (0.8)			NS (0.44)			NS (0.17)
			NS (0.67)			NS (0.44)			NS (0.7)
Complexity									
<50		NS (0.97)	**S (0.0001)**		NS (0.56)	**S (0.005)**		NS (0.55)	NS (0.33)
		NS (0.78)	NS (0.13)		NS (0.7)	NS (0.09)		NS (0.1)	NS (0.1)
50–60			NS (0.05)			NS (0.35)			NS (0.42)
			NS (0.07)			NS (0.87)			NS (0.65)
Coarseness									
<50		NS (0.19)	NS (0.08)		NS (0.56)	**S (0.004)**		NS (0.4)	NS (0.3)
		NS (0.37)	NS (0.3)		NS (0.5)	**S (0.01)**		NS (0.5)	NS (0.4)
50–60			NS (0.7)			**S (0.003)**			NS (0.2)
			NS (0.6)			**S (0.01)**			NS (0.08)
SS-TEL									
<50		NS (0.07)	NS (0.14)		**S (0.008)**	**S (0.0001)**		NS (0.83)	NS (0.71)
		NS (0.24)	NS (0.22)		**S (0.02)**	**S (0.04)**		NS (0.78)	NS (0.25)
50–60			NS (0.06)			NS (0.09)			NS (0.27)
			NS (0.2)			NS (0.11)			NS (0.09)
Entropy									
<50		NS (0.65)	NS (0.9)		NS (0.34)	NS (0.08)		NS (0.83)	**S (0.02)**
		NS (0.59)	NS (0.7)		NS (0.9)	NS (0.3)		S (0.81)	**S (0.04)**
50–60			NS (0.88)			NS (0.36)			NS (0.27)
			NS (0.5)			NS (0.7)			NS (0.4)
Thickness (mm)	0.42 ± 0.10	0.42 ± 0.10	0.42 ± 0.10	0.19 ± 0.11	0.26 ± 0.10	0.32 ± 0.13	0.61 ± 0.11	0.68 ± 0.10	0.74 ± 0.13
	0.41 ± 0.05	0.43 ± 0.12	0.46 ± 0.08	0.17 ± 0.09	0.26 ± 0.08	0.31 ± 0.12	0.59 ± 0.13	0.74 ± 0.18	0.82 ± 0.15

IL, intima layer; ML, media layer; IMC, intima–media complex. The p-value is shown in parentheses (S = significant difference at $p < 0.05$, NS = non significant difference at $p \geq 0.05$).

found a decrease of ML GSM with increasing age, as well as decrease with thickness (MLT), that can be attributed to the fact that, at the initial stages of atherosclerosis disease there is an increased concentration of lipids and hyperplasia of muscle fibers in the ML, which produces hypoechoic (echolucent) structures. It was also shown that the GSM of male patients is brighter than that of the female patients.

Similar to [13] we have also found that the IMT is generally larger in men than in women. Furthermore, in agreement with [12,15], we have also found that the IMT increases linearly with age.

In [23] increased IMT has been found in young adults with childhood-onset chronic kidney disease (CKD). The disease stage at which these patients first develop abnormalities of arterial texture is unknown. It was also shown that in 55 children with stages 2–4 CKD, thickening of IMT occurs early in the course of disease and is most prominently marked in dialyzed patients. Furthermore, morphologic alterations were found in both muscular and elastic type arteries as early as in the second decade of life. The degree of thickening depends on the degree of renal dysfunction. The authors also found that 61% of children with stages 2–4 CKD had IMT equal to or exceeding the 95th percentile for age.

It was shown in [3] that the GSM of the IM layer is the earliest change representing atherosclerotic disease in the arterial wall that can currently be imaged in vivo. This may be the first marker of atherosclerosis and may precede the development of significant increase in IMT. This would enable earlier identification of high-risk individuals based on the analysis of the CCA artery wall textural characteristics.

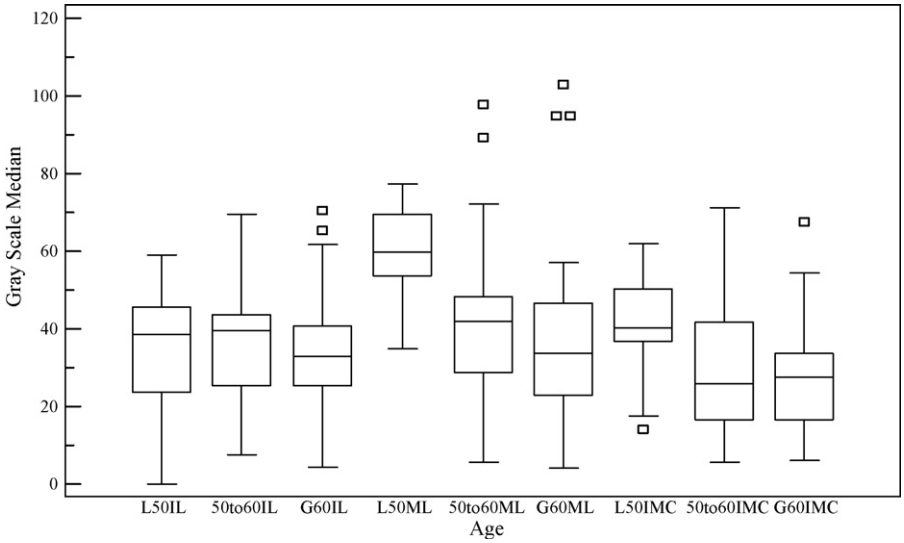

Fig. 2. Box plots of the gray-scale-median (GSM) texture feature extracted from IL, ML and IMC. Here we are using automated segmentations. In our description we let IQR denote the inter-quartile distance. From left to right, for the first three plots we have: L50IL for the IL for patients younger than 50 (IQR = 22), 50–60 IL for the IL for patients from 50 to 60 years old (IQR = 18.4), and G60IL for the IL for patients who are older than 60 years old (IQR = 15.4). For the next three plots (middle), we have the same age groups for the ML and IQR values of 16, 19.5 and 23.7 respectively. The last three plots (leftmost) show the GSM values for the IMC with IQR values 13.6, 25.2 and 16.9 respectively. In each plot we display the median, lower, and upper quartiles and confidence interval around the median of the GSM. Straight lines connect the nearest observations with 1.5 of the inter-quartile range (IQR) of the lower and upper quartiles. Unfilled rectangles indicate possible outliers with values beyond the ends of the 1.5× IQR.

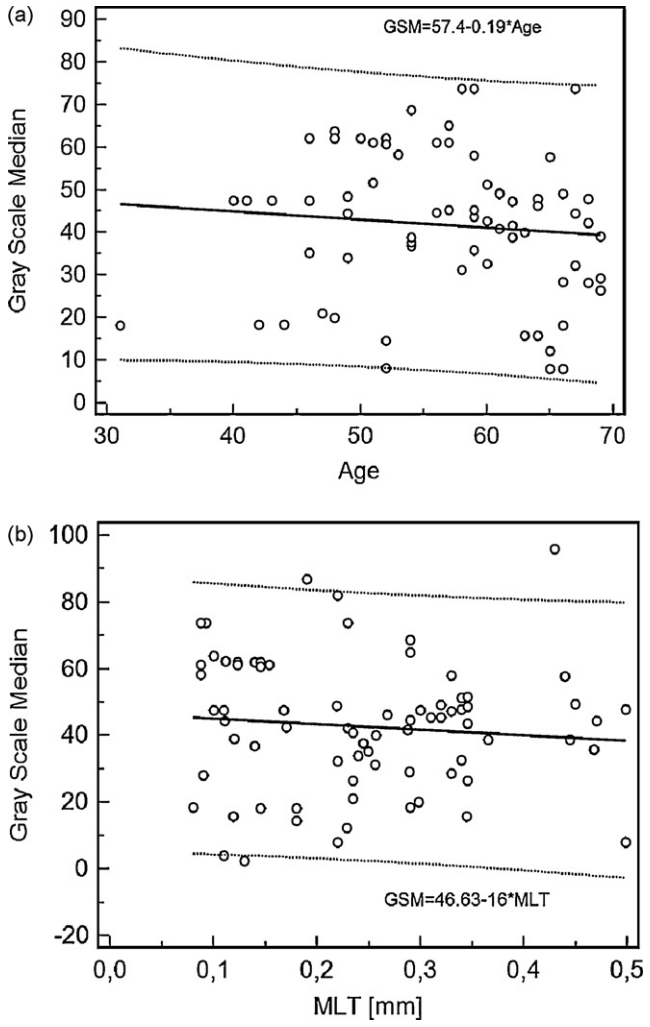

Fig. 3. Decrease of the GSM of the ML with (a) age, with a correlation coefficient $\rho = 0.12$ and (b) with MLT, with a correlation coefficient $\rho = 0.22$.

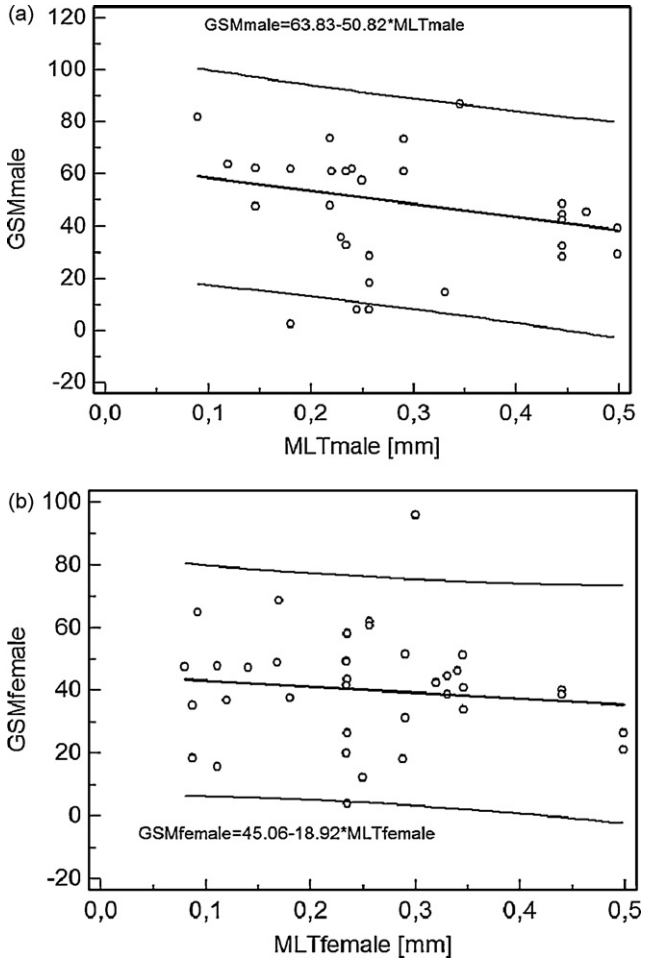

Fig. 4. Decrease of GSM for increasing MLT (a) male with a correlation coefficient $\rho = -0.29$ and (b) female patients, with a correlation coefficient $\rho = -0.13$.

Table 5
Statistical texture differences associated with gender. We used the Mann–Whitney rank sum to compare differences between male and female patients. The IL, ML, and IMC were automatically segmented. *P*-values are shown in parentheses.

Texture features	Automated		
	IL	ML	IMC
Mean	NS (0.62)	NS (0.71)	**S (0.04)**
Median (GSM)	NS (0.67)	NS (0.51)	**S (0.04)**
Stand. dev.	NS (0.46)	NS (0.81)	**S (0.03)**
Contrast	NS (0.24)	NS (0.85)	NS (0.83)
Difference var.	NS (0.57)	NS (0.52)	NS (0.92)
Complexity	NS (0.30	NS (0.55)	NS (0.23)
ASM	NS (0.63)	NS (0.70)	NS (0.14)
Coarseness	NS(0.61	NS (0.21)	NS (0.11)
SS-Text.E.L1	NS (0.57)	NS (0.34)	NS (0.17)
Entropy	NS (0.37)	NS (0.48)	**S (0.03)**
Periodicity	NS (0.33)	NS (0.45)	NS (0.7)
Diff. entropy	NS (0.12)	**S (0.04)**	**S (0.04)**
Sum variance	NS (0.8)	NS (0.78)	**S (0.04)**
Sum entropy	NS (0.4)	NS (0.67)	**S (0.02)**
Business	NS (0.5)	NS (0.77)	**S (0.04)**
Radial sum	NS (0.86)	NS (0.17)	**S (0.03)**

(S = significant difference at $p < 0.05$, NS = non significant difference at $p \geq 0.05$).

In [4], the texture features of 12 subjects (28 ± 2 years) with familial hypercholesterolemia (FCH) and without CVD, before and 3 months after treatment with atorvastatin were investigated, where the entropy and the ASM were extracted from the IMC band. Before treatment of atorvastatin significantly higher entropy (normal: 0.082 ± 0.02 vs FCH: 0.57 ± 0.12) and lower ASM (normal: 0.01 ± 0.0011 vs FCH: 0.004 ± 0.0001) values were found when compared to the normal tissue.

While IMT is an established measure of the vascular wall disease [2], GSM is less commonly used while other features have not been used before. GSM analysis has previously mainly been performed on plaques and then found to be related to histological features of the plaque, such as the elastin and calcium content, as well as to the size of the lipid-rich necrotic core [24]. However, the histological correlate to variation in the ML texture features has to be evaluated and the prognosis impact of these new variables has to be investigated. It has also been observed that there is an increase in the granularity in association with atherosclerotic disease [25]. A granular IMC indicates more advanced atherosclerosis, which may precede the development of significant IMT thickening.

5. Concluding remarks

In summary, our analysis showed that: (a) there are significant differences between some texture features extracted from the IL, ML and IMC (mean, gray scale median (GSM), standard deviation, contrast, difference variance, periodicity), (b) some of the texture features can be associated with the increase (difference variance, entropy) or decrease (GSM) of patient's age, (c) the GSM of the ML falls linearly with increasing ML thickness (MLT) and with increasing age, (d) the GSM of male subjects is larger than that of female subjects (see Fig. 4), and (e) male and female subjects may be better distinguished using texture features extracted form the IMC (see Table 5).

Future work will investigate whether it is possible to identify a group of patients at risk of atherosclerosis based on their texture features extracted from the IL, ML, and the IMC of high-resolution ultrasound images of the CCA. It may also be possible to identify and differentiate those individuals into high and low risk groups according to their cardiovascular risk before the development of plaques. The proposed methodology may also be applied to a group of people, which already developed plaques in order to study the contribution of the ML texture features to cardiovascular risk. Both groups of patients may benefit by prognosing and managing future cardiovascular events. Another possible future application of the proposed methodology is that it can be used to investigate possible effects of statins or other drugs in texture feature changes of the ML of the CCA.

References

[1] American Heart Association. Heart disease and stroke statistics-2007, update. Dallas, Texas; 2007.
[2] Pignoli P, Tremoli E, Poli A, Oreste P, Paoletti R. Intima plus media thickness of the arterial wall: a direct measurement with ultrasound imaging. Atherosclerosis 1986;74(6):1399–406.
[3] Ellis SM, Sidhu PS. Granularity of the carotid artery intima–medial layer: reproducibility of quantification by a computer-based program. BJOR 2000; 37:595–600.
[4] Bartolomucci F, Paterni M, Morizzo C, Kozakova M, et al. Early structural changes of carotid artery in familial hypercholesterolemia. J Clin Hypertens 2001;14:125A–6A.
[5] Lind L, Andersson J, Roenn M, Gustavsson T. The echogenecity of the intima–media complex in the common carotid artery is closely related to the echogenecity in plaques. Atherosclerosis 2007;195:411–4.
[6] Mario CD, Gorge G, Peters R, Pinto F, et al. Clinical application and image interpretation in coronary ultrasound. Study group of intra-coronary imaging of the working group of coronary circulation and of the subgroup of intravascular ultrasound of the working group of echocardiography of the European Society of Cardiology. Eur Heart J 1998;19:201–29.
[7] Grønhold ML, Nordestgaard BG, Schroeder TV, Vorstrup S, Sillensen H. Ultrasonic echolucent carotid plaques predict future strokes. Circulation 2001; 104(1):68–73.
[8] Gussenhoven EJ, Frietman PA, van Suylen SHRJ, van Egmond FC, Lancee CT, van Urk H, Roelandt JR, Stijnen T, Bom N. Assessment of medial thinning in atherosclerosis by intravascular ultrasound. Am J Cardiol 1991;68:1625–32.
[9] Loizou CP, Pattichis CS, Pantziaris M, Nicolaides A, Georgiou N, Kyriakou E. Media thickness measurement of the common carotid artery. In: 29th Conference Proceedings of IEEE in Engineering in Medicine and Biology Society. 2007. p. 2171–4.
[10] Loizou CP, Pattichis CS, Nicolaides AN, Pantziaris M. Manual and automated intima thickness measurements of the common carotid artery. IEEE Trans Ultrason Ferroelectr Freq Control. Accepted.
[11] Christodoulou CI, Pattichis CS, Pantziaris M, Nicolaides A. Texture-based classification of atherosclerotic carotid plaques. IEEE Trans Med Imaging 2003; 22(7):902–12.
[12] Prevention of disampling and fatal strokes by successful carotid endarterectomy in patients without recent neurological symptoms: randomized control trial. J Lancet 2004;363(9420):1491–502.
[13] Rosfors S, Hallerstam S, Jensen-Urstad K, Zetterling M, Carlstroem C. Relationship between intima–media thickness in the common carotid artery and atherosclerosis in the carotid bifurcation. Stroke 1998;29:1378–82.
[14] Balasundaram JK, Wahida Banu RSD. A non-invasive study of alterations of the carotid artery with age using ultrasound images. Med Biol Eng Comput 2006;44:767–72.
[15] Graf S, Gariery J, Massonneau M, Armentano R, et al. Experimental and clinical validation of arterial diameter waveform and intimal media thickness obtained from B-mode ultrasound image processing. Ultrasound Med Biol 1999;25(9):1353–63.
[16] Loizou CP, Pattichis CS, Pantziaris M, Tyllis T, Nicolaides A. Snakes based segmentation of the common carotid artery intima–media. Med Biol Eng Comput 2007;45:35–49.
[17] Tegos TJ, Sabetai MM, Nicolaides AN, Elatrozy TS, Dhanjil S, Stevens JM. Patterns of brain computed tomography infraction and carotid plaque echogenecity. J Vasc Surg 2001;33:334–9.
[18] Williams DJ, Shah M. A fast algorithm for active contour and curvature estimation. GVCIP: Image Understand 1992;55(1):4–26.
[19] Haralick RM, Shanmugam K, Dinstein I. Texture features for image classification. IEEE Trans Syst Man Cyber 1973;SMC-3:610–21.
[20] Weszka JS, Dyer CR, Rosenfield A. A comparative study of texture measures for terrain classification. IEEE Trans Syst Man Cyber 1976;SMC-6:269–85.
[21] Amadasun M, King R. Textural features corresponding to textural properties. IEEE Trans Syst Man Cyber 1989;19(5):1264–74.
[22] Wu CM, Chen YC, Hsieh K-S. Texture features for classification of ultrasonic images. IEEE Trans Med Imaging 1992;11:141–52.
[23] Litwin M, Wuehl E, Jourdan C, Trelewicz J, Niemirska A, Fahr K, Jobs K, Grena R, Wawer ZT, Rajszys P, Troeger J, Mehls O, Shaefer F. Altered morphological properties of large arteries in children with chronic renal failure and after and after renal transplantation. J Am Soc Nephrol 2005;16:1494–500.
[24] Goncalves I, Lindholm MW, Pedro LM, et al. Elastin and calcium rather than collagen or lipid content are associated with echogenecity of human carotid plaques. Stroke 2004;35(2):795–800.
[25] Belcaro G, Barsotti A, Nicolaides AN. Ultrasonic biopsy: a non-invasive screening technique to evaluate the cardiovascular system and to follow up the progression of atherosclerosis. Vascular 1991;20:40–50.

Christos P. Loizou is an assistant professor in computer science. He received his BSc degree in electrical engineering, the Dipl.-Ing. (MSc) degree in computer science and telecommunications from the University of Kaisserslautern, Kaisserslautern, Germany, and the PhD degree from the department of computer science, Kingston University, London, UK on ultrasound image analysis of the carotid artery in 1986, 1990 and 2005 respectively. From 1996 to 2000, he was a Lecturer in the department of computer science, Higher Technical Institute, Nicosia, Cyprus. Since 2000, he is an assistant professor in the department of computer science of the school of sciences and engineering, Intercollege, Cyprus. He has also served as a manager of a telecommunications company from 1990–1996. He has served as a supervisor of a number of PhD and BSc students in the area of computer image analysis and telemedicine. He has published 1 book, several journal and conference papers in the fields of image and video analysis. His current research interests include medical imaging and processing, motion and video analysis, signal and image processing, pattern recognition, biosignal analysis, in ultrasound, Magnetic Resonance, and Optical Coherence Tomography imaging and computer applications in medicine. Dr. Loizou is a member of the IEEE and a Senior Member of the IEE. He is also an associated researcher at the Institute of Neurology and Genetics in Nicosia, Cyprus. He serves as a reviewer, in many IEEE Transaction journals and served as a chair and co-chair, in many IEEE conferences. He received funding through different research projects supported by the Institute of Promotion and Foundation in Cyprus, which exceeds 1,700,000 Euros. His research work has been supported by various research grants and has been published in international conference proceedings and journals.

Marios Pantziaris received the MD degree in neurology from the Aristotelion University, Thessaloniki, Greece, in 1995. Currently, he is working with Cyprus Institute of Neurology and Genetics, Nicosia, Cyprus, as a Senior Neurologist in the Neurological Department and is the Head of the Neurovascular Department. He has been trained in Carotid Duplex–Doppler ultrasonography at St. Mary's Hospital, London, in 1995. In 1999, he was a visiting doctor in acute stroke treatment at Massachusetts General Hospital, Harvard University, Boston. He has considerable experience in carotids–transcranial ultrasound, has participated in many research projects, and has several publications to his name. He is also the Head of the Multiple Sclerosis (MS) Clinic where he is running research projects towards the aetiology and therapy of MS.

Marios S. Pattichis is an associate professor with the Department of Electrical and Computer Engineering and an Associate Professor with the Department of Radiology at the University of New Mexico (UNM), Albuquerque, New Mexico. His research interests are in the areas of medical image and video processing, digital image and video models, radar image processing, SIMD, and reconfigurable computer architecture applications. He is an associate editor for Pattern Recognition. At UNM, he received the 2004 ECE distinguished teaching award and the 2006 School of Engineering Harrison Faculty Recognition Award. He is a Senior Member of IEEE.

Efthyvoulos Kyriacou is an associate professor, at the Department of Computer Science and Engineering, Frederick University Cyprus. Undergraduate and Graduate studies at the department of Electrical & Computer Engineering of the National Technical University of Athens (NTUA) Greece (Diploma in Electrical and Computer Engineering 1996, PhD 2000). During the period 1996 to 2008 he was involved in a number of collaborations in both Greece and Cyprus. Research postgraduate student at the Institute of Communication and Computer Systems – NTUA (Feb. 1996–June 2000), working in the area of telemedicine, medical imaging and medical informatics. The Athens Medical Center Group in Athens Greece, working in the fields of telemedicine and medical databases (Sept. 2000–Oct. 2001). Visiting lecturer at the Dep. of Computer Science of the University of Cyprus (Sept. 2002–Dec. 2006). Postdoctoral researcher at the Cyprus Institute of Neurology and Genetics, working in the fields of medical image processing and medical informatics (Dec. 2001–Aug. 2006). Assistant Professor at Frederick institute of Technology (Jan. 2007–Sept. 2008). Since September 2008 he holds the position of Associate Professor in the Department of Computer Science and Engineering of Frederick University. He has published several journal and conference papers in the fields of telemedicine, medical imaging and medical informatics. He serves as an Associate Editor of the IEEE Trans. on Information Technology in Biomedicine (2007). He is a member of IEEE EMB and Computer Societies and the Hellenic society of Biomedical Engineering. His research interests focus on Telematics, image processing, neural networks and their applications in medicine.

Constantinos S. Pattichis received his diploma as technician engineer from the Higher Technical Institute in Cyprus, the BSc in electrical engineering from the University of New Brunswick, Canada, the MSc in Biomedical Engineering from the University of Texas at Austin, the MSc in Neurology from the University of Newcastle Upon Tyne, UK, and the PhD in electronic engineering from the University of London, UK. He is an associate professor with the Department of Computer Science of the University of Cyprus and a Senior Scientist of the Department of Computational Intelligence of the Cyprus Institute of Neurology and Genetics. His current research interests include health telematics, medical imaging, biosignal analysis and computational intelligence systems in medicine and in bioinformatics. He has been involved in numerous projects related to health telematics funded by EU and other bodies, like the AMBULANCE, EMERGENCY, ACSRS, TELEGYN, HEALTHNET, IASIS, IPPOKRATIS, and other with a total funding managed approaching 2 million Euros. He has published 7 chapters in books, 33 refereed journal and 95 conference papers in these areas. He is Co-Editor of the forthcoming book M-Health: Emerging Mobile Health Systems, to be published by Springer Science in 2005. He was Guest Co-Editor of the Special Issue on Emerging Health Telematics Applications in Europe of the IEEE Transactions on Information Technology in Biomedicine (TITB), and Chairman of the Medical and Biological Engineering and Computing Conference 98, and the IEEE MELECON 2000. He served as chairman of the IEEE Cyprus Section, and the Cyprus Society of Biomedical Engineering and Medical Physics. He serves as Associate Editor of the IEEE TITB, IEEE TNN and is a Senior Member of the IEEE.